DAVID W. TAYLOR NAVAL SHIP
RESEARCH AND DEVELOPMENT CENTER

Bethesda, Maryland 20084-5000

MEASURED SIMILARITY PROPERTIES OF EDDY VISCOSITY AND MIXING LENGTH IN THREE-DIMENSIONAL TURBULENT STERN FLOWS

by

Thomas T. Huang

APPROVED FOR PUBLIC RELEASE; DISTRIBUTION IS UNLIMITED.

Presented at the
Second International Symposium on Ship
Viscous Resistance 1985, SSPA
Göteborg, Sweden
18-20 March 1985

SHIP PERFORMANCE DEPARTMENT
RESEARCH AND DEVELOPMENT REPORT

May 1985

DTNSRDC-85/038

MEASURED SIMILARITY PROPERTIES OF EDDY VISCOSITY AND MIXING LENGTH
IN THREE-DIMENSIONAL TURBULENT STERN FLOWS

MAJOR DTNSRDC ORGANIZATIONAL COMPONENTS

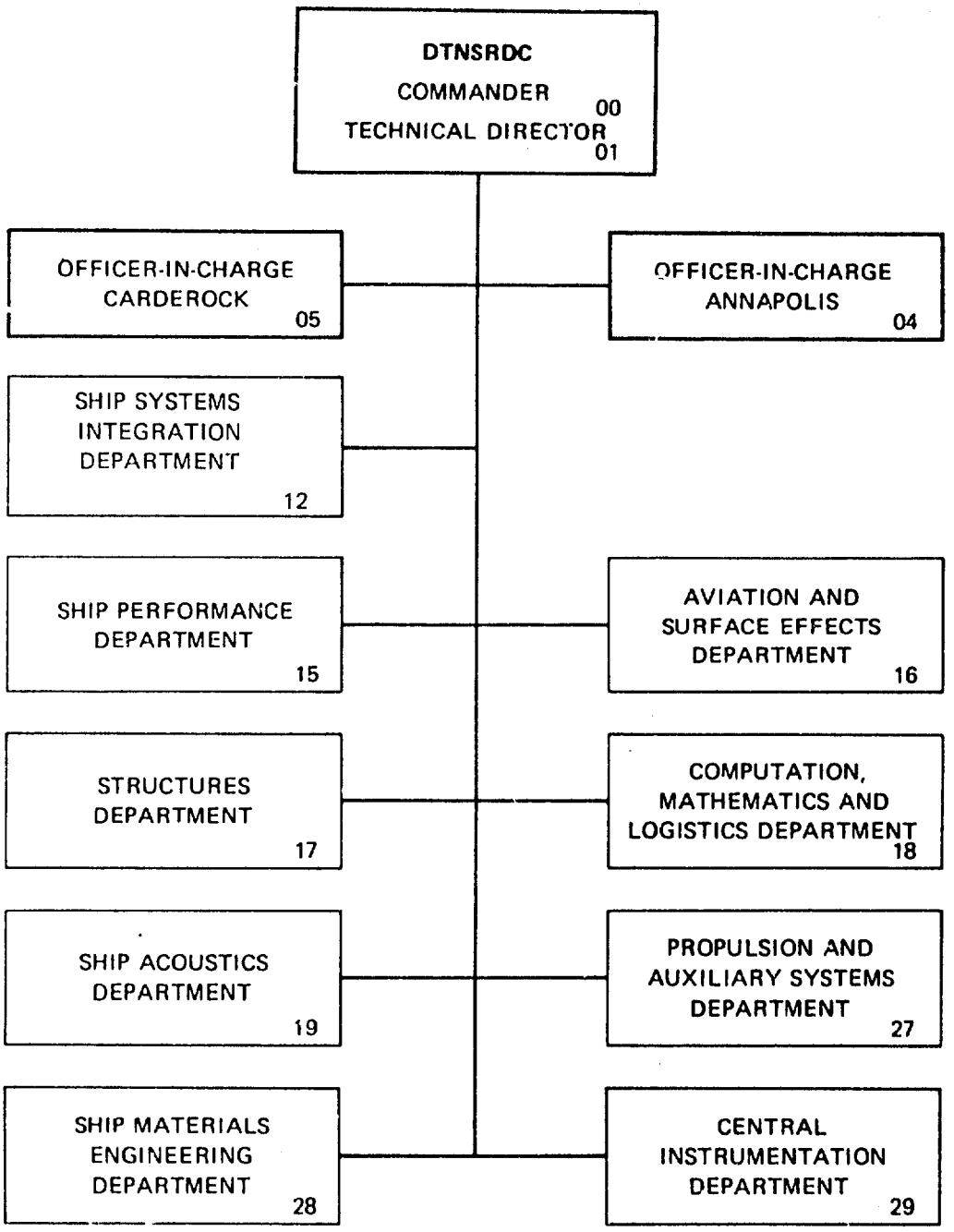

UNCLASSIFIED

SECURITY CLASSIFICATION OF THIS PAGE

REPORT DOCUMENTATION PAGE

1a REPORT SECURITY CLASSIFICATION UNCLASSIFIED	1b RESTRICTIVE MARKINGS
2a SECURITY CLASSIFICATION AUTHORITY	3 DISTRIBUTION / AVAILABILITY OF REPORT APPROVED FOR PUBLIC RELEASE; DISTRIBUTION IS UNLIMITED.
2b DECLASSIFICATION / DOWNGRADING SCHEDULE	
4 PERFORMING ORGANIZATION REPORT NUMBER(S) DTNSRDC-85/038	5 MONITORING ORGANIZATION REPORT NUMBER(S)
6a NAME OF PERFORMING ORGANIZATION David W. Taylor Naval Ship R and D Center 6b OFFICE SYMBOL (If applicable) 1542	7a NAME OF MONITORING ORGANIZATION
6c ADDRESS (City, State, and ZIP Code) Bethesda, Maryland 20084-5000	7b ADDRESS (City, State, and ZIP Code)
8a NAME OF FUNDING / SPONSORING ORGANIZATION 8b OFFICE SYMBOL (If applicable)	9 PROCUREMENT INSTRUMENT IDENTIFICATION NUMBER
8c ADDRESS (City, State, and ZIP Code)	10 SOURCE OF FUNDING NUMBERS PROGRAM ELEMENT NO: 61152N; PROJECT NO:; TASK NO: ZR0230101; WORK UNIT ACCESSION NO:

11 TITLE (Include Security Classification)
MEASURED SIMILARITY PROPERTIES OF EDDY VISCOSITY AND MIXING LENGTH IN THREE-DIMENSIONAL TURBULENT STERN FLOWS

12 PERSONAL AUTHOR(S)
Thomas T. Huang

13a TYPE OF REPORT	13b TIME COVERED	14 DATE OF REPORT (Year, Month, Day)	15 PAGE COUNT
Final	FROM _____ TO _____	1985 May	31

16 SUPPLEMENTARY NOTATION
Presented at the Second International Symposium on Ship Viscous Resistance 1985, SSPA Göteborg, Sweden, 18-20 March 1985

17 COSATI CODES			18 SUBJECT TERMS (Continue on reverse if necessary and identify by block number)
FIELD	GROUP	SUB-GROUP	Thick turbulent stern flows, turbulence modeling, eddy viscosity, mixing length.

19 ABSTRACT (Continue on reverse if necessary and identify by block number)

A comprehensive set of experimental turbulence data is presented for the stern region of simple three-dimensional models having 1:1, 2:1, and 3:1 elliptic transverse cross sections. Direct measurements of Reynolds stresses, turbulence kinetic energy, and mean velocity profiles are made by "X" hot-film anemometry. The values of eddy viscosity and mixing length are obtained from the measured Reynolds stresses and the mean velocity gradient. The experimentally-determined distributions of eddy viscosity and mixing length in the thick stern boundary layers are found to be smaller than values which have been proposed for thin boundary layers. Because eddy viscosity and mixing length models play an important role in stern boundary-layer calculations, a revised empirical mixing length model, which is assumed to be proportional to the square-root of the effective turbulence area, is proposed. The similarity properties of eddy viscosity and mixing

(Continued on reverse side)

20 DISTRIBUTION / AVAILABILITY OF ABSTRACT	21 ABSTRACT SECURITY CLASSIFICATION
☒ UNCLASSIFIED UNLIMITED ☐ SAME AS RPT ☐ DTIC USERS	UNCLASSIFIED
22a NAME OF RESPONSIBLE INDIVIDUAL Dr. Thomas T. Huang	22b TELEPHONE (Include Area Code) (202) 227-1325 22c OFFICE SYMBOL Code 1542

DD FORM 1473, 84 MAR 83 APR edition may be used until exhausted
All other editions are obsolete

SECURITY CLASSIFICATION OF THIS PAGE
UNCLASSIFIED

UNCLASSIFIED
SECURITY CLASSIFICATION OF THIS PAGE

REPORT DOCUMENTATION PAGE

1a REPORT SECURITY CLASSIFICATION UNCLASSIFIED	1b. RESTRICTIVE MARKINGS
2a SECURITY CLASSIFICATION AUTHORITY	3 DISTRIBUTION / AVAILABILITY OF REPORT APPROVED FOR PUBLIC RELEASE; DISTRIBUTION IS UNLIMITED.
2b DECLASSIFICATION / DOWNGRADING SCHEDULE	
4 PERFORMING ORGANIZATION REPORT NUMBER(S) DTNSRDC-85/038	5 MONITORING ORGANIZATION REPORT NUMBER(S)
6a NAME OF PERFORMING ORGANIZATION David W. Taylor Naval Ship R and D Center 6b OFFICE SYMBOL (If applicable) 1542	7a. NAME OF MONITORING ORGANIZATION
6c ADDRESS (City, State, and ZIP Code) Bethesda, Maryland 20084-5000	7b. ADDRESS (City, State, and ZIP Code)
8a NAME OF FUNDING / SPONSORING ORGANIZATION 8b. OFFICE SYMBOL (If applicable)	9. PROCUREMENT INSTRUMENT IDENTIFICATION NUMBER
8c ADDRESS (City, State, and ZIP Code)	10 SOURCE OF FUNDING NUMBERS PROGRAM ELEMENT NO. 61152N; PROJECT NO; TASK NO. ZR0230101; WORK UNIT ACCESSION NO

11 TITLE (Include Security Classification)
MEASURED SIMILARITY PROPERTIES OF EDDY VISCOSITY AND MIXING LENGTH IN THREE-DIMENSIONAL TURBULENT STERN FLOWS

12 PERSONAL AUTHOR(S)
Thomas T. Huang

13a TYPE OF REPORT	13b TIME COVERED	14. DATE OF REPORT (Year, Month, Day)	15. PAGE COUNT
Final	FROM _____ TO _____	1985 May	31

16 SUPPLEMENTARY NOTATION
Presented at the Second International Symposium on Ship Viscous Resistance 1985, SSPA Göteborg, Sweden, 18-20 March 1985

17 COSATI CODES		
FIELD	GROUP	SUB-GROUP

18. SUBJECT TERMS (Continue on reverse if necessary and identify by block number)
Thick turbulent stern flows, turbulence modeling, eddy viscosity, mixing length.

19 ABSTRACT (Continue on reverse if necessary and identify by block number)

A comprehensive set of experimental turbulence data is presented for the stern region of simple three-dimensional models having 1:1, 2:1, and 3:1 elliptic transverse cross sections. Direct measurements of Reynolds stresses, turbulence kinetic energy, and mean velocity profiles are made by "X" hot-film anemometry. The values of eddy viscosity and mixing length are obtained from the measured Reynolds stresses and the mean velocity gradient. The experimentally-determined distributions of eddy viscosity and mixing length in the thick stern boundary layers are found to be smaller than values which have been proposed for thin boundary layers. Because eddy viscosity and mixing length models play an important role in stern boundary-layer calculations, a revised empirical mixing length model, which is assumed to be proportional to the square-root of the effective turbulence area, is proposed. The similarity properties of eddy viscosity and mixing

Count keywords include:

(Continued on reverse side)

20 DISTRIBUTION / AVAILABILITY OF ABSTRACT	21. ABSTRACT SECURITY CLASSIFICATION
☒ UNCLASSIFIED/UNLIMITED ☐ SAME AS RPT ☐ DTIC USERS	UNCLASSIFIED

22a NAME OF RESPONSIBLE INDIVIDUAL	22b TELEPHONE (Include Area Code)	22c. OFFICE SYMBOL
Dr. Thomas T. Huang	(202) 227-1325	Code 1542

DD FORM 1473, 84 MAR — 83 APR edition may be used until exhausted. All other editions are obsolete.

SECURITY CLASSIFICATION OF THIS PAGE
UNCLASSIFIED

(Block 19 Continued)

length can be incorporated into the three-dimensional boundary layer computation methods using simple turbulence modeling or can be used as an initial input to the two-equation (k-ε) turbulence modeling method. The measured turbulence structural parameters $\overline{-u'v'}/(2K)$ and $\nu_t/(\sqrt{k}\ell)$ are found to be almost constant across the entire thick stern boundary layer. The measured proportionality constants are in agreement with those derived from the near-wall turbulence. The distributions of turbulence kinetic energy k and the turbulence energy dissipation ε can be approximately estimated once the distributions of mixing length ℓ and hence the eddy viscosity $\nu_t = \partial u_x/\partial n$ and the dominant Reynolds stress $\overline{-u'v'} = \nu_t\ \partial u_x/\partial n$ are known, where $\partial u_x/\partial n$ is the primary velocity gradient of the flow.

TABLE OF CONTENTS

A-1

LIST OF FIGURES

ADMINISTRATIVE INFORMATION

The work described in this paper was funded under the David W. Taylor Naval Ship Research and Development Center's Independent Research Program, Program Element 61152N, Task Area ZR0230101, and Work Unit 1542-103.

MEASURED SIMILARITY PROPERTIES OF EDDY VISCOSITY AND MIXING LENGTH IN THREE-DIMENSIONAL TURBULENT STERN FLOWS

T. T. HUANG
David W. Taylor Naval Ship Research & Development Center
Navy Dept., BETHESDA, Maryland 20084, USA

ABSTRACT

A comprehensive set of experimental turbulence data is presented for the stern region of simple three-dimensional models having 1:1, 2:1, and 3:1 elliptic transverse cross sections. Direct measurements of Reynolds stresses, turbulence kinetic energy, and mean velocity profiles are made by "X" hot-film anemometry. The values of eddy viscosity and mixing length are obtained from the measured Reynolds stresses and the mean velocity gradient. The experimentally-determined distributions of eddy viscosity and mixing length in the thick stern boundary layers are found to be smaller than values which have been proposed for thin boundary layers. Because eddy viscosity and mixing length models play an important role in stern boundary-layer calculations, a revised empirical mixing length model, which is assumed to be proportional to the square-root of the effective turbulence area, is proposed. The similarity properties of eddy viscosity and mixing length can be incorporated into the three-dimensional boundary layer computation methods using simple turbulence modeling or can be used as an initial input to the two-equation (k-ε) turbulence modeling method. The measured turbulence structural parameters $-\overline{u'v'}/(2K)$ and $\nu_t/(\sqrt{k}\ell)$ are found to be almost constant across the entire thick stern boundary layer. The measured proportionality constants are in agreement with those derived from the near-wall turbulence. The distributions of turbulence kinetic energy k and turbulence energy dissipation ε can be approximately estimated once the distributions of mixing length ℓ and hence the eddy viscosity $\nu_t = \partial u_x/\partial n$ and the dominant Reynolds stress $-\overline{u'v'} = \nu_t\, \partial u_x/\partial n$ are known, where $\partial u_x/\partial n$ is the primary velocity gradient of the flow.

NOTATION

A	Van Driest's damping factor (see Equation 6)
A(x)	Gross turbulence area, $A(x)/\pi = [(a+0.6\delta_a)(b+0.6\delta_b) - (a+\epsilon_a)(b+\epsilon_b)]$
a,b	Length of the major and minor elliptical axes at a given x/L, respectively
C_μ	Constant used in k-ε turbulence modeling, generally $C_\mu = 0.09$
k	Turbulence kinetic energy $(k = (u'^2 + v'^2 + w'^2)/2)$
L	Total body length
ℓ	Mixing length parameter (see Equation 6)
n,ζ	Coordinate measured normal and tangent to the body profile in the yz plane, respectively (Fig. 1)
r	Transverse radius of curvature
r_o	Radial distance for an axisymmetric body
r_t	Transverse radius of curvature of the body
U_δ	Inviscid flow velocity at the edge of the boundary layer
U_i	Axial component of the inviscid flow velocity at the body surface
U_o	Free-stream velocity
U_x	Axial component of the inviscid flow velocity

Second International Symposium on Ship Viscous Resistance 1985
SSPA Maritime Consulting AB
P O Box 24001, S 40022 GÖTEBORG, Sweden

u_x, v_n, w_θ Mean velocity components in the x, n, and θ directions, respectively

$\sqrt{\overline{(u')^2}}$, $\sqrt{\overline{(v')^2}}$, $\sqrt{\overline{(w')^2}}$ Turbulent fluctuations in the x, n, and θ direction, respectively

$\overline{u'v'}$, $\overline{u'w'}$ Reynolds stresses

$-\overline{u'v'}/(2k)$ Turbulence structural parameter

x,y,z Orthogonal body coordinates (Fig. 1)

γ_t Intermittancy Factor, $\gamma_t = [1 + 5.5\ (\frac{n}{\delta})^6]^{-1}$

δ_a, δ_b Boundary-layer thicknesses along the a and b axes, respectively

δ_r Boundary-layer thickness measured in the n direction

δ_p^* Planar displacement thickness (see Equation 5)

δ_{995} Boundary-layer thickness at which $u_x/U_x = 0.995$

ϵ Turbulent dissipation (see Equation 3)

θ Angular coordinate measure in the y-z plane

$\overline{\theta}$ Angle between the x and θ coordintes

$\lambda^*=\lambda u^*/\nu$ Generalized Van Driest damping factors

λ Length parameter related to Van Driest damping factors

ν Kinematic viscosity of the fluid

$\nu_t/(\sqrt{k}\ell)$ Non-dimensional turbulence structure parameter

ν_t Eddy viscosity (see Equations 1 and 6)

ρ Mass density of the fluid

τ_w Wall shear stress

1. INTRODUCTION

The turbulent flow characteristics in a ship's stern region are of particular interest to naval architects since many single-screw propellers operate inside thick boundary layers. An accurate prediction of velocity inflow to the propeller is essential to meet the ever-increasing demand for improved wake-adapted propeller performance. The integral and/or differential methods used to predict turbulent boundary-layer characteristics agree well with experimental data in thin boundary layers. However, predictions from these methods deviate from measured values as the boundary layer thickens. Often, the boundary layer is thicker than the transverse dimension of the model in the stern region, nullifying the basic assumption that the boundary layer is small when compared with model dimensions. It is hoped that some insight into the flow in this complex region can be gained through detailed measurements of the turbulent boundary-layer characteristics in the stern region of simple geometries. To minimize the variables associated with three dimensionality, models with 2:1 and 3:1 elliptic cross sections were designed to have the same longitudinal distributions of cross-sectional area as one of the axisymmetric models tested [Axisymmetric Model 1] in Reference 1. Previous investigations at the David W. Taylor Naval Ship Research and Development Center have produced comprehensive sets of experimental data for pressure, shear stress, velocity, and turbulence across the sterns of three axisymmetric models [1, 2], and two three-dimensional models having 3:1 and 2:1 elliptic transverse cross sections [3, 4]. These experimental data reveal three distinctive features of the thick stern boundary-layer flows: (1) strong viscous/inviscid interaction, (2) significant cross-stream pressure variation, and (3) special mixing length/eddy viscosity with a distinct "zonal" turbulence structure. The data for simple three-

dimensional models having 1:1, 2:1, and 3:1 elliptic transverse cross sections [1,3,4] are used to show the special turbulence characteristics of the stern flows.

In the following sections, the models and experimental techniques are given in detail. The measurements of mean velocities, turbulence intensities, and Reynolds stresses are analyzed to obtain eddy viscosity and mixing length. The measured turbulent kinetic energy k, and the derived eddy viscosity ν_t, the mixing length ℓ, and the turbulent dissipation ε are presented to demonstrate that the thick turbulent stern flows possess a distinct "zonal" turbulence structure.

2. MODELS AND EXPERIMENTAL TECHNIQUES

The detailed offsets of Axisymmetric Model 1 are given in Table 1. The bow-entrance length/diameter ratio, parallel middle body length/diameter and afterbody length/diameter ratio of this model are 1.82, 4.85, and 4.31, respectively. The total length of the model is 3.066-m (10.06-ft.). The diameter of the parallel middle body (r_{max}) is 13.97-cm (0.458-ft). The longitudinal distributions of the transverse cross sectional areas of the 2:1 and 3:1 elliptic models are equal to those of the Axisymmetric Model 1. Thus, the three models have the same volume and longitudinal distribution of buoyancy. However, the 2:1 and 3:1 elliptic models have 9% and 23% more wetted surface area, respectively, than the axisymmetric model. A schematic of the three sterns, together with the flow measurement stations, is shown in Fig. 1.

The experimental investigation was conducted in the DTNSRDC Anechoic Flow Facility. The wind tunnel has a closed jet test section that is 2.4-m (8-ft) square and 4.19-m (13.75-ft) long. The corners have fillets which are carried through the contraction. The test section is followed by an acoustically lined large chamber, 7.17-m (23.5-ft) long. It was found previously by Huang et al. [1] that the ambient free-stream turbulence levels are 0.075, 0.090, and 0.100, and 0.12 ~ 0.15 for free-stream velocities U_o of 24.4, 30.5, 38.1, and 45.7 m/s, respectively. Integration of the measured noise spectrum levels in the test section from 10 to 10,000 Hz indicated that the typical background acoustic noise levels at 30.5 m/s were about 93 dB re 0.0002 dyne/cm^2 (0.0002 Pa). These levels of ambient turbulence and acoustic noise were considered low enough so as not to unfavorably affect the measurement of boundary-layer characteristics. The maximum air speed that can be achieved is 61 m/s (200 ft/sec); in the present experiments, the wind tunnel velocity was held constant at 30.48 m/s.

The models were supported either by three streamlined guide wires with one streamlined strut located downstream of the model or by two streamlined struts separated by one-third of the model length. The disturbances generated by the supporting struts were within the region below the horizontal centerplane. All the measurements were made in each model's vertical centerplane along the upper meridian, where there was little extraneous effect from the supporting struts. The aft one-half of the model length protruded beyond the closed-jet section into the open-jet section. The ambient static pressure coefficients across and along the entire open-jet chamber (7.2 m x 7.2 m x 6.4 m) were found to vary by less than 0.3% of the dynamic pressure. Tunnel blockage and longitudinal pressure gradient effects along the tunnel length were almost completely removed by testing the afterbody in the open-jet section. The two three-dimensional models are shown in the Anechoic Wind Tunnel Facility in Figure 2. The location of the boundary-layer transition from laminar to turbulent flow was artificially induced by a 0.61-mm (0.024-in)-diam trip wire located at x/L = 0.05. Flow visualization techniques using oil dots identified a small region of flow separation on the two three-dimensional sterns. The turbulent flow separation on the 3:1 model was found to begin at x/L = 0.90 and to reattach at x/L = 0.98. The maximum lateral extent of the separation region occurred at x/L = 0.94 and covered a region of $80° \leq \theta \leq 90°$. The measured boundary layer cross flow was found to be quite large ($w/U_o \cong 0.1$) at $\theta = 80°$ upstream of the separation. The smaller separation region on the 2:1 model began at x/L = 0.94 and reattached at x/L = 0.96. The lateral extent of the separation region at x/L = 0.95 was around $83° \leq \theta \leq 90°$. No separation was found on the stern of Axisymmetric Model 1.

The mean axial and radial velocities and the turbulence intensities for the Reynolds stress calculations were measured by a TSI, Inc., Model 1241-20 "X" type hot-film probe. The probe elements are 0.05 mm (0.002 in.) in diameter with a sensing length of 1.0 mm (0.04 in.). The spacing between the two cross elements is 1.0 mm (0.04 in.). A two-channel hot-wire and hot-film anemometer with linearizers was used to monitor the response of the hot-film probe. A temperature-compensating sensor (probe) was used with each hot-film element to regulate the operating temperature of the sensor with changes in air temperature. The "X" hot-film and its temperature-compensated sensor were calibrated together through the expected

air temperature range and supplied with their individual linearization polynomial coefficients at the factory.

For reliable measurements, the frequency response of the anemometer system is claimed by the manufacturer to be 0-100 kHz. Calibration of the "X" hot-film probe was made immediately before and after each set of measurements. The maximum deviation of the hot-film output from the mean linear response curve was held to within 0.5% of the free-stream velocity. In addition, the standard deviation of the hot-film measurements of the free-stream velocity at 45.72 m/s (150 ft/sec) at the reference location were recorded before and after an experimental series and were held to within 0.5%. An estimate was made of the cross-flow velocity by yawing the "X" hot-film probe at the reference free-stream location. It was found that the measured cross-flow velocities were about 1% of the free-stream velocity. At 10 randomly selected points across the thick boundary layer, the streamwise and cross-flow velocity components were measured at five different times. The standard deviations of the streamwise and cross-flow velocity components were found to be less than 1% and 2%, respectively.

The linearized signals were fed into a Time/Data Model 1923-C real-time analyzer. Both channels of the analog signal were digitized at a rate of 128 points per second for 8 seconds. These data were immediately analyzed by a computer to obtain the individual components of mean velocity, turbulence fluctuation, and Reynolds stress on a real-time basis.

A traversing system with a streamlined strut was mounted on a guide plate that permitted the traverse to be locked into various stationary positions parallel to the longitudinal model axis.

All data are presented in the coordinate system used to experimentally measure the boundary-layer flows. The coordinate system, denoted by x-n-θ, is given in Fig. 1. The axial coordinate x is measured from the nose of the body and passes through the center of the elliptic profile. The coordinates n and θ are defined along an axial cut normal to the x axis, i.e., in the yz plane. The normal component n is measured from the model surface and is normal to the elliptic surface but not to the model as a whole. The angular coordinate θ is defined as the angle, in degrees, measured from the z-minor axis to the line joining the surface offset and elliptic center.

Mean velocity and turbulence measurements were taken with an "X" hot-film sensor which was stepped away from the body in the n direction. Measurements of velocity in the axial x and normal n directions, u_x and v_n, respectively, were taken with the probe elements aligned vertically. The sensor elements were rotated 90° to the horizontal position to measure the mean velocity w_θ in the θ direction. An on-line computer was used to collect data at a sample rate of 1024 data values in 8 sec. The root-mean square values of turbulence velocity were recorded at each probe position, and the eddy viscosity and mixing length values were computed from the measured Reynolds stresses and the measured mean velocity profiles.

The distribution of the Reynolds stresses $-\overline{u'v'}$, $-\overline{u'w'}$, $\overline{(u')^2}$, $\overline{(v')^2}$, and $\overline{(w')^2}$ represent the turbulence characteristics in the thick boundary layer. The mean-square turbulent velocity fluctuations $\overline{(u')^2}$ in the axial direction and $\overline{(v')^2}$ in the n direction, and the Reynolds stress $-\overline{u'v'}$ were measured with the "X" hot-film probe elements aligned vertically. The probe elements were rotated 90° to the horizontal position to measure both the turbulent fluctuation $\overline{(w')^2}$ in the θ direction and the Reynolds stress $-\overline{u'w'}$.

Linear interpolation was used to approximate $\overline{(w')^2}$ and $-\overline{u'w'}$ at the same off-body positions as the data measured in the vertical direction.

3. MEASURED AND DERIVED TURBULENT CHARACTERISTICS OF THICK STERN FLOWS

The measured and derived turbulent characteristics relevant to the analysis of thick stern boundary-layer flows are presented below.

3.1 Measured Reynolds Stresses

The typical turbulence characteristics in the thick boundary layer can be represented by the distributions of Reynolds stresses, namely, $-\overline{u'v'}$, u'^2, where u', v', and w' are the turbulent velocity fluctuations in the axial, radial, and azimuthal directions, respectively. Figure 3 shows the measured distribution of Reynolds stress $-\overline{u'v'}/U_o^2$ and three components of turbulence intensity at several axial locations along the 1:1 afterbody. In general, for a given location, the intensity of the axial turbulent-velocity component has the highest value and the intensity of the radial component has the smallest value. The degree of anisotropy decreases as the stern boundary layer becomes thicker. Furthermore, the increased boundary-layer thickness is accompanied by a reduction of turbulence intensities in the inner region. The variation along the body of the radial location of the maximum values of the measured Reynolds stress $-\overline{u'v'}/U_o^2$ layer is small. The spatial resolution of the cross-wire probe is not fine enough to measure the Reynolds stress distribution in the inner region when the boundary layer is thin. As the stern boundary layer increases in thickness, the location of maximum Reynolds stress moves away from the wall (Figure 3). The values of Reynolds stress $-\overline{u'v'}$ decrease quickly from the maximum value to zero at the edge of the boundary layer. As shown in Figure 3, the shape of the Reynolds stress distribution curves in the outer region is quite similar for all the thick boundary layers. It is interesting to note that the shapes of the measured Reynolds stresses in the inner regions of the near wake at x/L = 1.057 and 1.182 experience a drastic reduction in magnitude.

3.2 Measured Turbulence Kinetic Energy k

The measured turbulence kinetic energy $k = (\overline{u'^2} + \overline{v'^2} + \overline{w'^2})/2$ is shown in Figure 4. The thin boundary layer can be seen in the region of $x/L < 0.8$ of the 1:1 model and as the large flat portions of the 2:1 and 3:1 models, $\theta < 60°$. The maximum value of k measured in this region occurs very close to the wall (less than 10% of the boundary-layer thickness) and the measured value of k decreases almost linearly towards the edge of the boundary layer. However, the measured k in the inner region of the thick boundary layer has a constant value for almost 60% of the boundary-layer thickness. The distinct characteristics of the measured values of k in the thick boundary layer are found in Fig. 5 for $x/L > 0.9$ for the 1:1 model and in the corner region of the major axis ($75° < \theta < 90°$) of the 2:1 and 3:1 models.

3.3 Derived Eddy Viscosity, Mixing Length, Turbulence Kinetic Energy Dissipation

The values of eddy viscosity and mixing length are not measured directly but are obtained, as in previous studies [1-4] from the measured values of the Reynolds stress $-\overline{u'v'}$ and the mean velocity gradient $\partial u_x/\partial n$. The definitions used to compute these quantities are

$$-\overline{u'v'} = \nu_t \frac{\partial u_x}{\partial n} = \ell^2 \left\{ \left(\frac{\partial u_x}{\partial n}\right)^2 + \left(\frac{\partial w_\theta}{\partial n}\right)^2 + 2\left(\frac{\partial u_x}{\partial n}\right)\left(\frac{\partial w_\theta}{\partial n}\right)\cos\bar{\theta} \right\}^{1/2} \frac{\partial u_x}{\partial n} \qquad (1)$$

When the values of w_θ/U_x are less than 0.1 and $\bar{\theta}$, the angle between the coordinates x and θ (Fig. 1) is 90° for the present measurements, Equation (1) may be approximated by

$$-\overline{u'v'} = \nu_t \frac{\partial u_x}{\partial n} = \ell^2 \frac{\partial u_x}{\partial n} \qquad (2)$$

A spline curve is used to fair the experimental data before the velocity gradient is obtained numerically. The dissipation of the turbulence kinetic energy is

$$\varepsilon = \nu \overline{\frac{\partial u_i'}{\partial x_k} \frac{\partial u_i'}{\partial x_k}} \tag{3}$$

$$= \nu \left\{ \overline{\left(\frac{\partial u'}{\partial x}\right)^2} + \overline{\left(\frac{\partial v'}{\partial x}\right)^2} + \overline{\left(\frac{\partial w'}{\partial x}\right)^2} + \overline{\left(\frac{\partial u'}{\partial n}\right)^2} + \overline{\left(\frac{\partial v'}{\partial n}\right)^2} + \overline{\left(\frac{\partial w'}{\partial n}\right)^2} \right.$$

$$\left. + \overline{\left(\frac{\partial u'}{\partial \zeta}\right)^2} + \overline{\left(\frac{\partial v'}{\partial \zeta}\right)^2} + \overline{\left(\frac{\partial w'}{\partial \zeta}\right)^2} \right\}$$

It is necessary to measure each of the above nine mean-square derivatives to determine accurately the value of ε. Because of the practical limitations of hot-wire techniques and the tremendous time required to measure even a few of the nine terms, a direct measurement of the value of ε was not attempted. However, by dimensional analysis of k and ε, one finds

$$\nu_t = C_\mu \frac{k^2}{\varepsilon} \tag{4}$$

where the constant $C_\mu = 0.09$ is recommended by Launder et al. [5,6], and is generally accepted in the community of k-ε turbulence modeling. Since the values of k, $-\overline{u'v'}$, and u_x (hence $\partial u_x/\partial n$) were determined by direct measurements and the values of ν_t were derived from Equation (2), the values of ε can then be derived from Equation (4).

4. COMPARISON OF SIMPLE THIN BOUNDARY LAYER TURBULENCE MODELS WITH THE MEASURED DATA

The simple mixing length model of Bradshaw et al. [7] and the simple eddy viscosity model of Cebeci and Smith [8] are compared with the present measured data from the thick stern boundary layer.

4.1. Comparison of the Bradshaw et al. [7] Mixing Length Model With Present Data

When the past history of boundary layer characteristics is important, Bradshaw et al. [7] argue that the turbulence energy equation can be used to model the "memory" effect. In order to determine the rate of change of the shear stress along a mean streamline, three assumptions are made: namely, (1) the local Reynolds stress $-\overline{u'v'}/(2k) = 0.15$; (2) the dissipation rate is determined by the local Reynolds stress and a length scale depending on n/δ_T, and; (3) the energy diffusion is directly proportional to the local Reynolds stress with a factor depending on the maximum value of the Reynolds stress. On the basis of thin boundary-layer data, two empirical functions for the last two assumptions were proposed by Bradshaw et al. [7]. The first assumption $\ell/\delta = f_1\ (n_1\delta_T)$ can be evaluated by the present thick boundary layer data and is shown in Fig. 5. This assumption is found not to be applicable to thick stern flows. The measured values of ℓ/δ_T are much smaller (sometimes by a factor of 3) than those of the thin boundary layer.

It is important to note that the boundary-layer thickness of a typical body increases drastically at the stern. Most of the rapid change takes place within a streamwise distance of a few boundary-layer thicknesses. Most of the empirical functions for solving the turbulence energy equation will undergo rapid changes. The one known function is the empirical function for mixing length, as shown in Fig. 5, for defining the value of ℓ/δ_T as a function of n/δ_T. Therefore, the empirical functions used by Bradshaw et al. [7] need to be revised for the thick stern boundary layers.

4.2 Comparison of the Cebeci and Smith [8] Eddy Viscosity Model With Present Data

In most simple turbulence models, the basic assumption made in the differential methods for calculating turbulent boundary layers is that the Reynolds stress is modeled by the product of the mean velocity gradient and the eddy viscosity or the square of the mean velocity gradient and the mixing length. Both the eddy viscosity and the mixing length are uniquely related to the boundary-layer thickness parameter at the local station. As long as the boundary layer is thin and the change in boundary-layer properties due to the pressure gradient, and body geometry is gradual, this simple turbulence model is known to be satisfactory, (e.g. Cebeci and Smith [8]). The experimentally-determined distributions of eddy viscosity, $\nu_t/U_e\delta_p^*$, are shown in Fig. 6 for the three sterns, where δ_p^* is the displacement thickness, defined as

$$\delta_p^* = \int_o^{\delta_r} \left\{ 1 - \frac{u_x}{U_x} \right\} dn \qquad (5)$$

where n and δ are the distance and the boundary thickness, respectively, measured normal to the body surface and normal to the body axis, U_x is the value of the axial component of the inviscid flow velocity, and u_x is the axial inviscid velocity component. The generalized eddy viscosity model of Cebeci and Smith [8] for a three-dimensional body [9] is

$$\nu_t = \begin{cases} \nu_i \text{ for inner region, } 0 \leq n \leq n_c \\ \nu_o \text{ for outer region, } n_c \leq n \leq \delta_r \end{cases} \qquad (6)$$

where

$$\nu_i = \begin{cases} \ell_i^2 \left[\left(\frac{\partial u_x}{\partial n}\right)^2 + \left(\frac{\partial w_\theta}{\partial n}\right)^2 + 2 \left(\frac{\partial u_x}{\partial n}\right)\left(\frac{\partial w_\theta}{\partial n}\right) \cos \bar{\theta} \right]^{1/2} \equiv \ell_i^2 \frac{\partial u_x}{\partial n} \\ \ell_i^2 \left(\frac{r}{r_o}\right)\left(\frac{\partial u_x}{\partial n}\right) \text{ for axisymmetric flow} \end{cases}$$

$$\ell_i = \begin{cases} 0.4\, n \left[1 - \exp\left(-\frac{n}{A}\right)\right] \\ 0.4\, r_o \ln\left(\frac{r}{r_o}\right) \left[1 - \exp\left[-\frac{r_o}{A} \ln \frac{r}{r_o}\right]\right] \text{ for axisymmetric flow} \end{cases}$$

$$\nu_o = 0.0168\, U_\delta\, \delta_p^*\, \gamma_{tr}$$

$$A = 26\nu\, (\tau_w/\rho)^{-1/2} = 26\nu/u_*, \text{ Van Driest damping factor}$$

$$\gamma_{tr} = \left[1 + 5.5\, (n/\delta_r)^6\right]^{-1}$$

δ_r = δ_{995}, boundary layer thickness at which $u_x/U_x = 0.995$

τ_w = wall shear stress

As shown in Figure 6a, the measured distributions of eddy viscosity agree reasonably well with the eddy viscosity of Cebeci and Smith [8] when the boundary layers are thin. However, as the stern boundary layer thickens, the measured values of $\nu_t/U_\delta \delta_p^*$ in the thick stern boundary layer shown in Fig. 6 are significantly (as much as one order of magnitude) smaller than the values for thin boundary layers given by the Cebeci and Smith model. Therefore, this commonly-used, simple turbulence model of Cebeci and Smith for thin boundary layers is not suitable for thick boundary layers.

5. "ZONAL" TURBULENT SIMILARITY PROPERTIES OF THICK STERN FLOWS

The solutions of the time-dependent, three-dimensional, Navier-Stokes equations with adequate resolution of time and spatial scales by today's computers, are limited to laminar flows at very low Reynolds numbers. The time-averaged Navier-Stokes equations are often used to compute the mean flow quantities at high Reynolds numbers, but the time-dependent solutions are then sacrificed. The simplified time-averaged Reynolds equations require a set of closure relationships for Reynolds stresses. The closure relationship reduces the number of unknowns to the number of equations. The common approach to closure is to define an eddy viscosity (an artifice) for turbulent flows in the same form as the laminar viscosity in the stress tensor for the Newtonian flows. The specification of the eddy viscosity in terms of algebraic or differential equations has been the major area of turbulence research for the past 20 years. Some of the turbulence models are successful for thin boundary layers and for simple flows, but none of the closure relationships is universally valid for all complex flows. Therefore, Kline [10] in his summary of the 1980-81 Stanford Conference emphasized the importance of developing "zonal models" for various structural flow zones. Thick turbulent stern flows possess a special similarity flow structure which differs from that of thin boundary layers. These distinct "zonal" characteristics of turbulent stern flows are discussed below.

5.1. Similarity Property of Mixing Length for Turbulent Stern Flows

For three axisymmetric and two simple three-dimensional turbulent stern flows, Huang et al. [1,2,3,4] obtained a similarity property of the measured mixing length. The mixing

length was found to be proportional to the square root of the entire turbulence area between the body surface and the edge of the boundary layer. Although the apparent boundary layer thickens rapidly toward the stern, this turbulent area undergoes a relatively small change in the stern region. Therefore, the mixing length does not change appreciably in the stern region. As shown in Figures 3 and 4, the measured values of Reynolds stresses and turbulent kinetic energy k in the thick stern boundary layer decrease from a relatively large value at 60 percent of the boundary layer thickness to zero at the outer edge of the boundary layer. Contrary to the thin boundary layer data, the measured values of k in the thick boundary layer remain almost constant within 60 percent of the boundary-layer thickness (Fig. 4). An approximate correlation of the measured contours of non-dimensional turbulence kinetic energy $\sqrt{k}/U_o$ and the measured contours of the boundary-layer thickness for the 2:1 model is shown in Fig. 7. The measured contour of $0.6\delta_r$ is very close to the measured contour of $\sqrt{k}/U_o = 0.04$. Within the contour of $0.6\delta_r$ and the body surface, the measured values of $\sqrt{k}/U_o$ are found to vary from 0.035 to 0.055 for all the data taken for the three models. The measured values of $\sqrt{k}/U_o$ reduce rapidly to about 0.01 at the edge of the boundary layer.

For axisymmetric and simple three-dimensional elliptic sterns, the gross turbulence area $A(x)/\pi \equiv [(a+0.6\delta_a)(b+0.6\delta_b) - (a+\varepsilon_a)(b+\varepsilon_b)]$, may be more relevant to the mixing length parameter, where ε_a and ε_b are the effective thickness of the separation bubble (to allow for low turbulence mixing) in the direction of the major and minor axes, a and b, respectively, of the elliptical cross-section, and δ_a and δ_b are the boundary-layer thicknesses along the a and b axes. A small separation bubble (covering $0.90 \leq x/L \leq 0.98$ for the 3:1 model and $0.92 \leq x/L \leq 0.96$ for the 2:1 model) was detected in the corner region of the major axis, and the values of ε_a are found to be negligibly small. The flow does not separate from the entire flat portion of the two elliptic sterns along the minor axis ($\varepsilon_b = 0$). For the axisymmetric stern $a=b=r_o$, $\delta_a=\delta_b=\delta_r$, and $\varepsilon_a = \varepsilon_b = 0$ (the flow remained attached over the entire body for axisymmetric models tested). The similarity property of the mixing length ℓ for the turbulent stern flows can be evaluated by plotting $\ell/\sqrt{A/\pi}$ versus n/δ_r, where n is the distance normal to the body surface and the longitudinal axis δ_r is the boundary-layer thickness in the n-direction, taken as the value of n at which $u_x/U_x = 0.995$, u_x is the viscous axial velocity and U_x is the inviscid axial velocity. At the location of δ_r, the measured value of $\sqrt{k}/U_o$ is about 0.01.

The normalized mixing length distributions for the three axisymmetric bodies investigated by Huang et al. [1,2] are shown in Figures 8a through 8c; Figures 8d through 8g show the distribution for the 2:1 model [4]; and Figures 8h through 8j show the distributions for the 3:1 model [3]. As shown in Figure 8, the measured values of the normalized mixing length are fairly similar over the entire thick boundary layer region of all the sterns. This similarity property remains valid even for the mild separation region of the elliptic models. The curve shown in Figure 8 is the average line of the data and can be represented by

$$\frac{\ell_o}{\sqrt{A/\pi}} = 0.169 \frac{n}{\delta_r} \exp\left[-\frac{6}{5}\frac{n}{\delta_r} - \frac{32}{30}\left(\frac{n}{\delta_r}\right)^3 \right] \qquad (7)$$

It is assumed that Equation (7) is approximately valid for an arbitrary three-dimensional stern. The boundary-layer thickness δ_r (and hence $0.6\delta_r$) can be obtained from most boundary-layer computation procedures. Therefore, a simple numerical evaluation can be performed to compute the effective turbulence area A/π for general three-dimensional stern flows.

It is important to note that when the boundary-layer thickness of the axisymmetric stern equals 23 percent of the transverse radius of curvature, $r_t=a=b=r_o=\delta_r/0.23$, Equation (7) becomes

$$\ell_o = 0.40\, n \exp\left[-\frac{6}{5}\frac{n}{\delta_r} - \frac{32}{30}\frac{n}{\delta_r}^3 \right] \qquad (8)$$

This relationship very closely resembles the empirical mixing length curve proposed by Bradshaw et al. [7]. As shown in Fig. 5a, Equation (8) obtains a maximum ℓ_o/δ_r value of 0.096 at $n/\delta_r = 0.5$. Since Equation (8) and the Bradshaw et al. empirical mixing

length curve are in good agreement, Equation (8) will be assumed valid for all thin boundary layers with the boundary layer thicknesses less than 23 percent of the transverse radii of curvature of the bodies.

Although Equations (7) and (8) specify the mixing length distribution for the entire thick and thin boundary layers, respectively, the classical mixing length (consistent with the logarithmic velocity laws) is more appropriate for the inner wall region. For example, the generalized mixing length proposed by Granville [11],

$$\ell_i = \frac{0.4y}{\sqrt{1+\left(\frac{y}{r_t}\right)}} \left[1 - \exp\left(-y^*/\lambda^*\right)\right] \tag{9}$$

where

$$\lambda^* = 26 + 1.36 \times 10^3 \frac{1}{r_t^*} + 2.73 \times 10^4 \left(\frac{1}{r_t^*}\right)^2$$

can be used, where r_t is the transverse radius of curvature, y is the distance normal to the wall, λ^* is the generalized Van Driest damping factor, $\lambda^*=\lambda u_*/\nu$, $r_t^*=r_t u_*/\nu$, $u_* = \sqrt{\tau_w/\rho}$ τ_w is the wall shear stress, ν is the kinematic viscosity, ρ is the mass density of the fluid, and λ is the length factor. Equation (9) reduces to the classical mixing length for the thin two-dimensional boundary layer when $r_t \to \infty$, e.g.,

$$\ell_i = 0.4y \left[1 - \exp(-y^*/26)\right] \tag{9a}$$

The value of ℓ_i increases almost linearly with increasing y for large values of y. In the outer boundary layer, the maximum value of the mixing length is limited by Equation (7) for the thick boundary layer and by Equation (8) for the thin boundary layer. At the intersection of the inner and the outer regions ($n=n_c$ shown in Fig. 9), the condition of $\ell_o=\ell_i$ must be applied. The shaded line shown in Fig. 9 is the proposed mixing length distribution across both the thick and thin boundary layers, and may be summarized as follows,

$$\ell_o = \begin{cases} \text{Equation (7) for thick boundary layer, } \delta_r \geq 0.23\ r_t \\ \text{Equation (8) for thin boundary layer, } \delta_r \leq 0.23\ r_t \end{cases} \quad \text{for outer region, } n \geq n_c \tag{10}$$

$$\ell_i = \text{Equation (9)} \quad \text{for inner region, } n \leq n_c$$

$$\text{and} \quad \ell_o = \ell_i \text{ at } n = n_c$$

The boundary layer is classified as thick when the boundary-layer thickness is equal to or greater than 23 percent of the transverse radius of the curvature of the body. For a small separation bubble at the stern, Equations (7) and (8) can still be applied outside of the separation bubble. However, Equation (9) gives $\ell_i=0$ at separation, due to $u_* = 0$, and, therefore, becomes an unnecessary inner region.

Existing thin boundary-layer methods are well developed and can be applied from the forward portion of the body to the location where the boundary-layer thickness increases to 23 percent of the radius of the transverse curvature of the body. Further downstream, the proposed similarity property of the thick stern boundary layer given by Equation (10) can be used to solve the turbulent stern flows. The presently proposed direct model for calculating ℓ (and hence ν_t and $-\overline{u'v'}$ by Equation (10)) without the need of solving a differential equation can be called a Zero-Equation Model.

5.2 Measured Turbulence Structural Parameters

In turbulence modeling, the non-dimensional turbulence structural parameters $-\overline{u'v'}/k$ and $\nu_t/(\sqrt{k}\ell)$ are often constant in the turbulent flow field. The proportionality constants obtained for the near-wall turbulence are assumed to be universal coefficients

and to be valid for general turbulent flows. These proportionality constants have been derived by Launder, et al. [5,6,12] as well as many others. A brief summary of the characteristics of the near-wall turbulence will be repeated and the proportionality constants obtained from the near-wall turbulence will be compared with the measured values for the entire thick stern flows.

Very near the wall, the stress $\overline{u_i'u_j'}$ is dominated by $\overline{u'v'}$; and the turbulent velocity fluctuations (with turbulence fluctuations u' in the primary flow direction x and v' in the primary velocity-gradient direction) are small, while the turbulence production and dissipation are large. Therefore, the advection term and the diffusion-loss term in the turbulence energy equation [7] can be neglected, e.g.,

$$\left[u_m \frac{\partial}{\partial x_m}\right] k - \frac{\tau}{\rho}\frac{\partial u_x}{\partial n} + \frac{\partial}{\partial n}\left[\overline{p'v'} + 1/2\ \overline{kv'}\right] + \nu \overline{\frac{\partial u_i'}{\partial x_m}\frac{\partial u_i'}{\partial x_m}} = 0$$

reduces to a balance of the turbulence energy production and dissipation, or

$$\frac{\tau}{\rho}\frac{\partial u_x}{\partial n} = \nu \overline{\frac{\partial u_i'}{\partial x_m}\frac{\partial u_i'}{\partial x_m}} = \varepsilon$$

Furthermore, the convective acceleration term and the longitudinal pressure gradient are usually much smaller than the normal shear stress gradient. Hence the mean flow momentum equation

$$\left[u_m \frac{\partial}{\partial x_m}\right] u_x = -\frac{1}{\rho}\left(\frac{\partial p}{\partial x}\right) + \frac{\partial}{\partial n}\left(\frac{\tau}{\rho}\right)$$

reduces to

$$\frac{\partial}{\partial n}\left(\frac{\tau}{\rho}\right) = 0$$

which means that

$$\frac{\tau}{\rho} = \nu\frac{\partial u_x}{\partial n} - \overline{u'v'} = \frac{\tau_w}{\rho} = u_*^2 \qquad (11)$$

or $$-\overline{u'v'} = u_*^2$$

if the small contribution of the laminar stress is neglected.
Using the definition of mixing length

$$-\overline{u'v'} = \ell^2\left(\frac{\partial u_x}{\partial n}\right)^2 = u_*^2$$

the approximated velocity gradient near the wall becomes

$$\frac{\partial u_x}{\partial n} = \frac{u_*}{\ell}$$

The approximated turbulence energy dissipation near the wall can be obtained as

$$\varepsilon = \frac{\tau}{\rho}\frac{\partial u_x}{\partial n} = -\overline{u'v'}\frac{\partial u_x}{\partial n} = \frac{u_*^3}{\ell} \qquad (12)$$

If the commonly used relationship of eddy viscosity $\nu_t = C_\mu k^2/\varepsilon$ (with $C_\mu = 0.09$) is applied, a very useful result is obtained, e.g.,

$$-\overline{u'v'} = \nu_t \frac{\partial u_x}{\partial n} = \frac{C_\mu k^2 \frac{\partial u_x}{\partial n}}{\varepsilon} = \frac{C_\mu k^2 \frac{\partial u_x}{\partial n}}{-\overline{u'v'}\frac{\partial u_x}{\partial n}}$$

or

Therefore, one of the proportionality constants of the turbulence structural parameter can be evaluated,

$$\frac{-\overline{u'v'}}{K} = \sqrt{C_\mu} \quad \text{or} \quad \frac{-\overline{u'v'}}{2k} = 0.15 \text{ (with } C_\mu = 0.09) \tag{13}$$

The other proportionality constant of the turbulence structural parameter is

$$\frac{\nu_t}{\sqrt{k}\ell} = \frac{C_\mu \frac{k^2}{\varepsilon}}{\sqrt{k}\ \ell} = \frac{C_\mu k^{3/2}}{\varepsilon \ell} = \frac{C_\mu \left(\frac{u_*^2}{\sqrt{C_\mu}}\right)^{3/2}}{u_*^3} = C_\mu^{1/4} = 0.548 \tag{14}$$

Here we have used the alternative turbulence structural parameter

$$\frac{k^{3/2}}{\varepsilon \ell} = \frac{\left(\frac{u_*^2}{\sqrt{C_\mu}}\right)^{3/2}}{u_*^3} = C_\mu^{-3/4} \tag{15}$$

The typical measured distributions of $-\overline{u'v'}/(2k)$ are shown in Fig. 10. The present thick stern flow data shown in Fig. 10 indicate that the measured values of $-\overline{u'v'}/(2k)$ are almost constant at an approximate value of 0.15 up to $0.6\delta_r$ and decrease towards the edge of boundary layer. It should be pointed out that the measured values of k include the contribution of free-stream turbulence, no attempt having been made to remove the free-stream turbulence from the measured values of k. The measured reduction of the proportionality constant near the outer edge of the boundary layer is in part caused by the larger contribution of the free-stream turbulence to k than to $-\overline{u'v'}$. Nevertheless, the measured values of the turbulence structure parameter of $-\overline{u'v'}/(2k)$ are quite constant and agree well with the proportionality constant of $-\overline{u'v'}/(2k) = 0.15$ derived from the near-wall turbulence (Equation (13)) within 60 percent of the boundary layer thickness, the region where the effect of free-stream turbulence is small.

The measured distributions of $\nu_t/(\sqrt{k}\ell)$ are shown in Fig. 11. The proportionality constant $\nu_t/(\sqrt{k}\ell)$, derived from the near-wall turbulence (Equation (14)), is 0.548. The present thick stern flow data shown in Fig. 11 indicate that the measured values of $\nu_t(\sqrt{k}\ell)$ are nearly constant for the entire boundary layer. The measured values of $\nu_t/(\sqrt{k}\ell)$ for 1:1 model agree very well with the proportionality constant of 0.548 derived from the near-wall turbulence. However, the measured values of $\nu_t/(\sqrt{k}\ell)$ for the 2:1 and 3:1 models are slightly lower than 0.548 and decrease slightly towards the edge of the thick boundary layer. The consistency of the measured values of $\nu_t/(\sqrt{k}\ell) \equiv C_\mu^{1/4} = 0.548$ across the entire thick boundary layer can be used to estimate the distribution of the turbulent kinetic energy, $k \equiv (\nu_t/\ell)^2 \sqrt{C_\mu}$ once the distribution of the values of ℓ and hence the values

of ν_t are known across the thick stern flow. Furthermore, the distribution of the turbulence energy dissipation can be estimated by $\varepsilon = C_\mu^{3/4} k^{3/2}/\ell = \nu_t^3/\ell^4$.

6. CONCLUSION

Direct measurements of Reynolds stresses, turbulence kinetic energy, and mean velocity profiles have been made by "X" hot-film anemometry for the stern region of simple three-dimensional models having 1:1, 2:1, and 3:1 elliptic transverse cross sections. The values of eddy viscosity and mixing length were obtained from the measured Reynolds stresses and the mean velocity gradients. The following conclusions can be drawn from the detailed analyses of the directly measured experimental data on the turbulence characteristics of thick stern flows.

The experimentally-determined distributions of eddy viscosity and mixing length in the thick stern boundary layers were found to be smaller than values which have been proposed for thin boundary layers. A special similarity property of mixing length for turbulent stern flows has been found. The mixing length in the outer region of the thick boundary layer(ℓ_o) is found to be proportional to the square-root of the effective turbulence area A/π, where A is the area between 60 percent of the boundary-layer thickness and body's surface. The mixing length distribution ℓ in the outer region is given by

$$\ell = \begin{cases} \ell_o = 0.169\sqrt{A/\pi}\ \dfrac{n}{\delta_r}\exp\left[-\dfrac{6}{5}\dfrac{n}{\delta_r} - \dfrac{32}{30}\left(\dfrac{n}{\delta_r}\right)^3\right] & \text{for thick B.L., } \delta_r > 0.23\, r_t \\ \ell_o = 0.4\, n \exp\left[-\dfrac{6}{5}\dfrac{n}{\delta_r} - \dfrac{32}{30}\left(\dfrac{n}{\delta_r}\right)^3\right] & \text{for thin B.L., } \delta_r < 0.23\, r_t \end{cases}$$

where n is the distance normal to the surface and the longitudinal axis and δ_r is the boundary-layer thickness in the n-direction, taken as the value of n at which the boundary layer velocity approaches 0.995 of the inviscid velocity. The classical mixing length (ℓ_i), consistent with the logarithmic velocity laws is more appropriate for the inner region (Equation (9)), where the conditions $\ell = \ell_i$ for $n \leq n_c$, $\ell = \ell_o$ for $n \geq n_c$ and $\ell_o = \ell_i$ at $n = n_c$ are imposed for the application of the revised mixing length model.

Across 60 percent of the thick stern boundary layer, the measured turbulence structural parameter, $-\overline{u'v'}/(2k)$ was found to be approximately 0.15, a value in agreement with $-\overline{u'v'}/(2k) = \sqrt{C_\mu}/2$ derived from the near-wall turbulence. Another measured turbulence structural parameter $\nu_t/(\sqrt{k}\ell)$, was found to be almost constant across the entire thick stern boundary layer. The proportionality constant for $\nu_t/(\sqrt{k}\ell)$, given by $C_\mu^{1/4} \cong 0.548$, was derived from the near-wall turbulence structure, and found to be approximately valid for the entire stern boundary layer. The consistency of these two measured turbulence structural parameters together with the definition of $\nu_t = C_\mu k^2/\varepsilon$ can be used to estimate the distribution of turbulence energy, $k = (\nu_t/\ell)^2/\sqrt{C_\mu}$, and the distribution of turbulence energy dissipation, $\varepsilon = \nu_t^3/\ell^4 = C_\mu^{3/4} k^{3/2}/\ell$ as long as the distributions of mixing length ℓ and hence the eddy viscosity ($\nu_t = \ell^2\, \partial u_x/\partial n$) are known across the entire thick boundary layer.

ACKNOWLEDGEMENTS

The experimental data described in this paper were obtained funded under the David W. Taylor Naval Ship Research and Development Center's Independent Research Program, Program Element 61152N, Task Area ZR0230101, DTNSRDC Work Unit 1542-103 (FY84).

The author would like to thank Mrs. Nancy Groves and Dr. Ming-Shun Chang, for their assistance in the preparation of this paper, which was supported by the General Hyrdomechanics Research Program of the Naval Sea Systems Command, Program Element 61153N, Task Area SR0230101, DTNSRDC Work Unit 1542-070.

REFERENCES

[1] Huang, T.T., N. Santelli, and G.S. Belt, "Stern Boundary-Layer Flow on Axisymmetric Bodies," 12th Symposium on Naval Hydrodynamics, Washington, D.C. (5-9 June 1978). Available from National Academy of Science, Washington, D.C., pp. 127-147, 1979

[2] Huang, T.T., N.C. Groves, and G.S. Belt, "Boundary-Layer Flow on an Axisymmetric Body with an Inflected Stern," DTNSRDC Report 80/064, 1980

[3] Groves, N.C., G.S. Belt, and T.T. Huang, "Stern Boundary-Layer Flow on a Three-Dimensional Body of 3:1 Elliptic Cross Section," DTNSRDC Report 82/022, 1982

[4] Huang, T.T., N.C. Groves, and G.S. Belt, "Stern Boundary-Layer Flow on a Three-Dimensional Body of 2:1 Elliptic Cross Section," DTNSRDC Report 84/022, 1984

[5] Launder, B.E., A. Morse, W. Rodi, and D.B. Spalding, "The Prediction of Free Shear Stress Flows - A Comparison of the Performance of Six Turbulence Models," Proc. Langley Free Shear Flows Conf. NASA SP 321, July 1972

[6] Launder, B.E., and G.J. Reece, and W. Rodi, "Progress in the Development of a Reynolds-Stress Turbulence Closure," J. Fluid Mech. Vol. 68, Part 3, pp. 537-577, 1975

[7] Bradshaw, P., D.H. Ferriss, and N.P. Atwell, "Calculation of Boundary Layer Development Using the Turbulent Energy Equation," J. Fluid Mech. Vol. 28, Part 3, pp. 593-616, 1967

[8] Cebeci, T. and A.M.O. Smith, "Analysis of Turbulent Boundary Layers," Academic Press, New York, 1974

[9] Cebeci, T., K.C. Chang, and K. Kaups, "A General Method for Calculating Three-Dimensional Laminar and Turbulent Boundary Layers on Ship Hulls," McDonnell Douglas Corp. Report J7998, 1978. Also Ocean Engineering, Vol. 7, pp. 229-289, Pergamon Press, Great Britain, 1980

[10] Kline, S.J., "Universal or Zonal Modeling - The Road Ahead," in Kline, S.J., B.J. Cantwell, and G.M. Lilley (Eds.): "1980-81 AFOSR-HTTM-Stanford Conference on Complex Turbulence Flows," Vol. II, pp. 991-1015, 1982

[11] Granville, P.S., "Mixing Lengths or Eddy Viscosities for Thick Axisymmetric Turbulent Boundary Layer Near a Wall," paper submitted to the ASME/ASCE Mechanics Conference, June 1985

[12] Hanjalic, K., and B.E. Launder, "Sensitizing the Dissipation Equation to Irrotational Strains," J. Fluid Engineering, Trans, ASME, Vol. 102, pp. 34-40, 1980

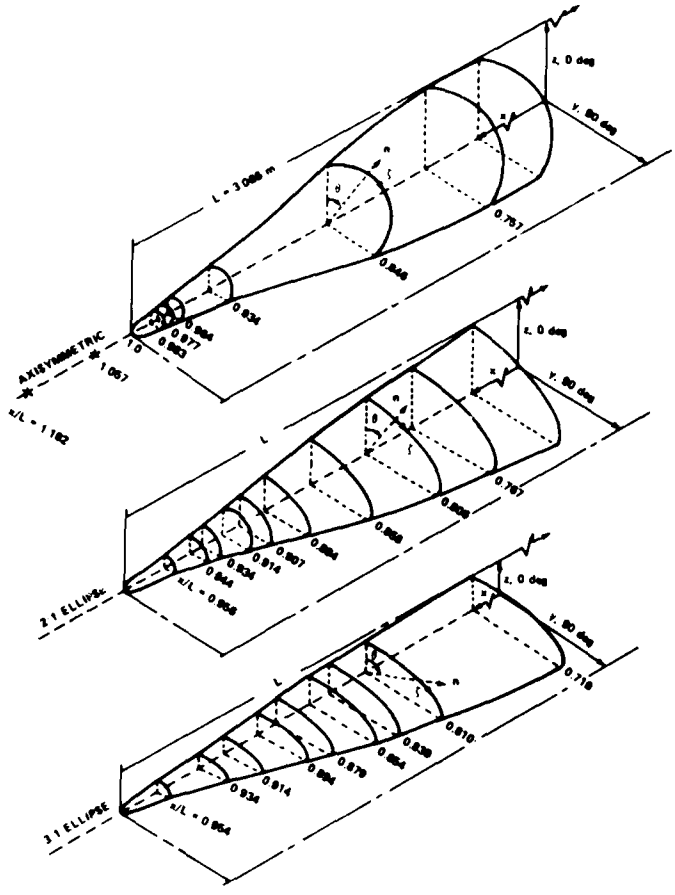

Figure 1 - Schematic of the Three Sterns Showing Measurement Stations

Figure 2 - Two Elliptic Models Mounted in a Wind Tunnel

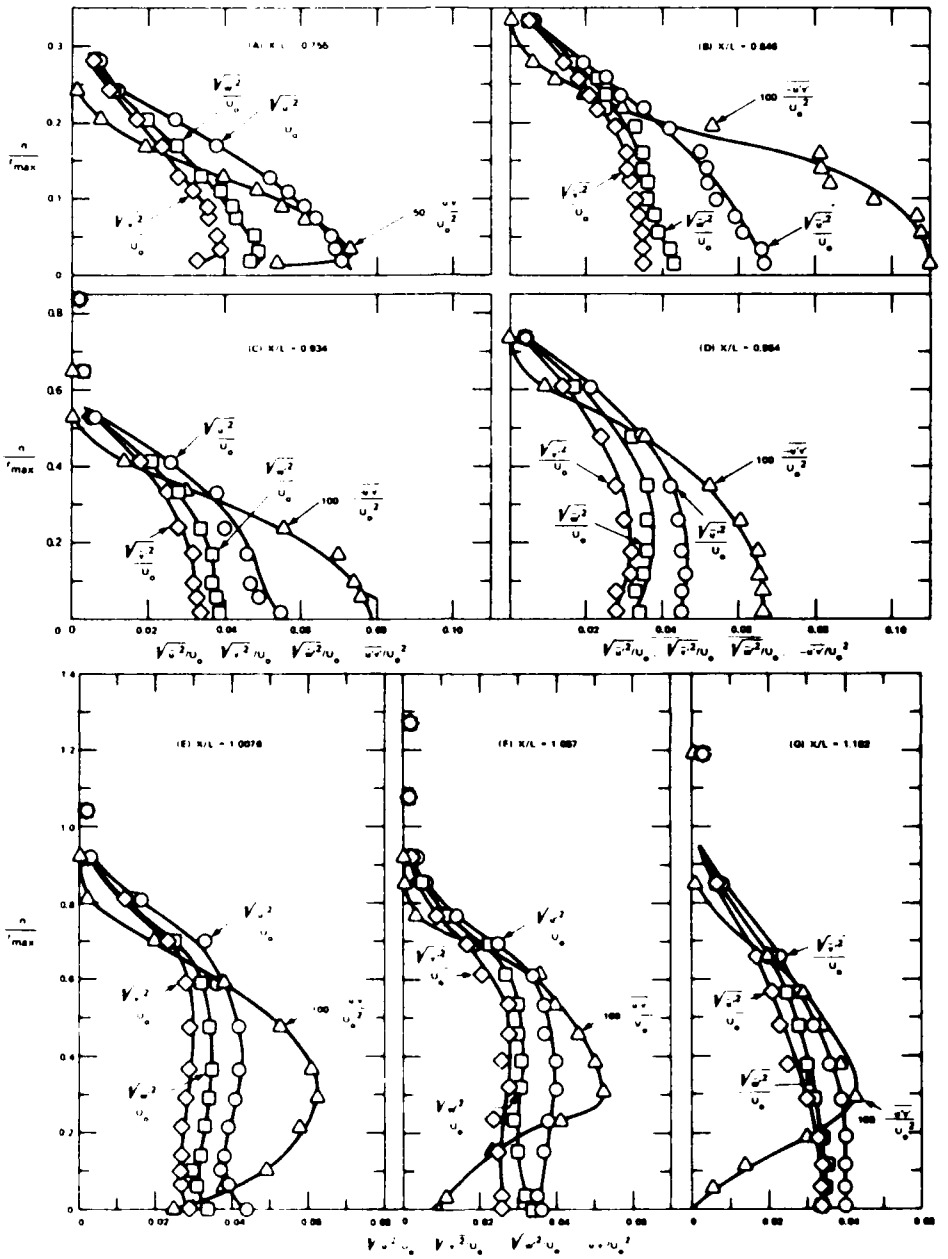

Figure 3 - Measured Distributions of Reynolds Stresses (Model 1:1)

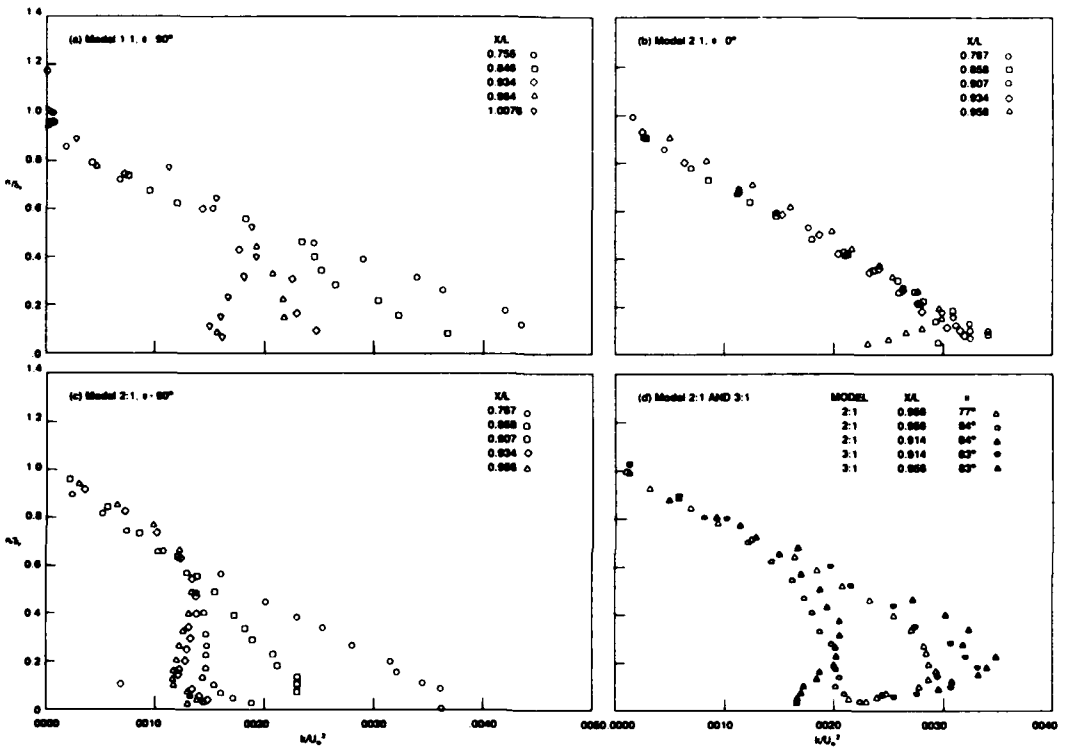

Figure 4 - Measured Turbulence Kinetic Energy

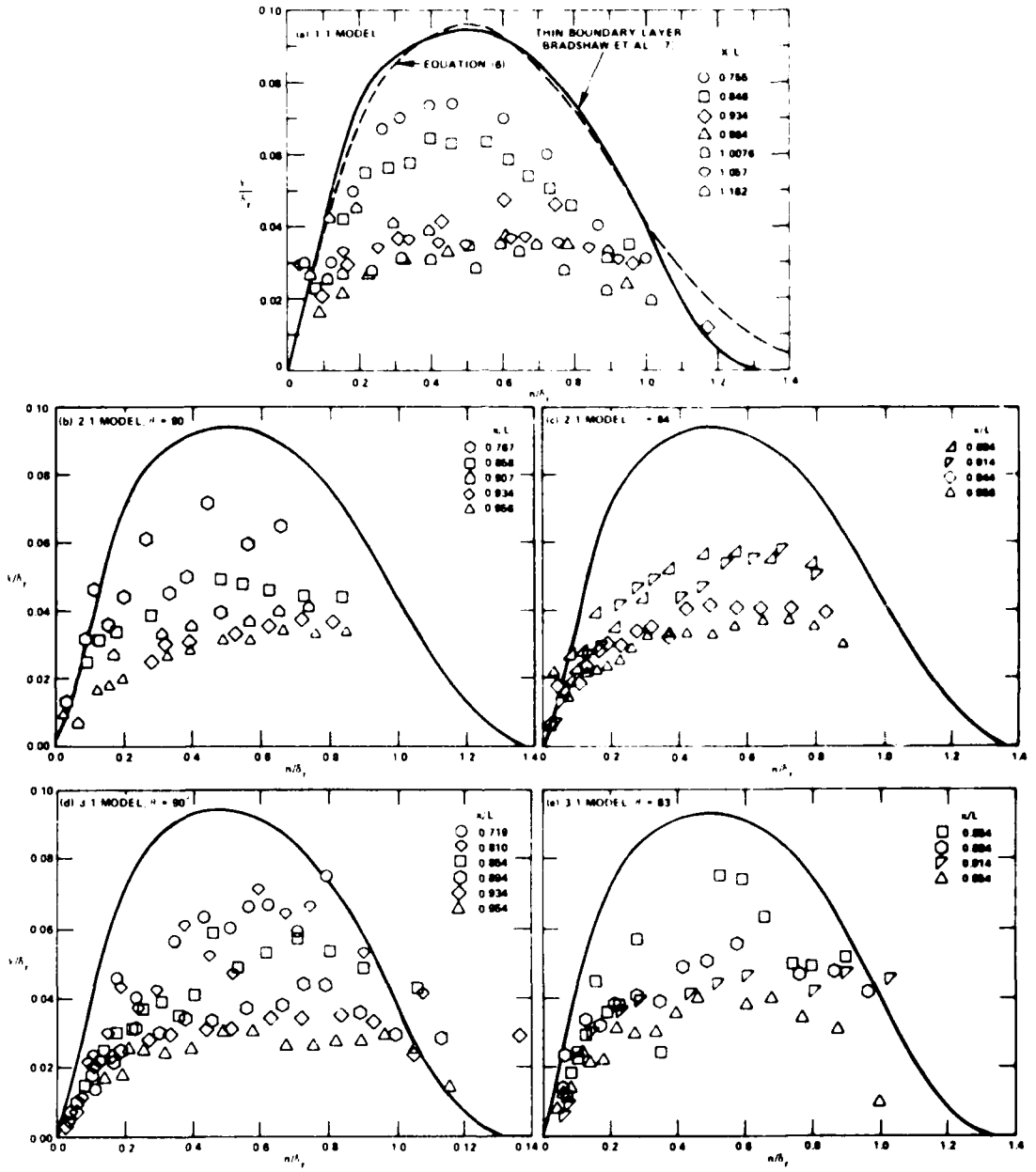

Figure 5 - Measured Distribution of Mixing Length Parameter

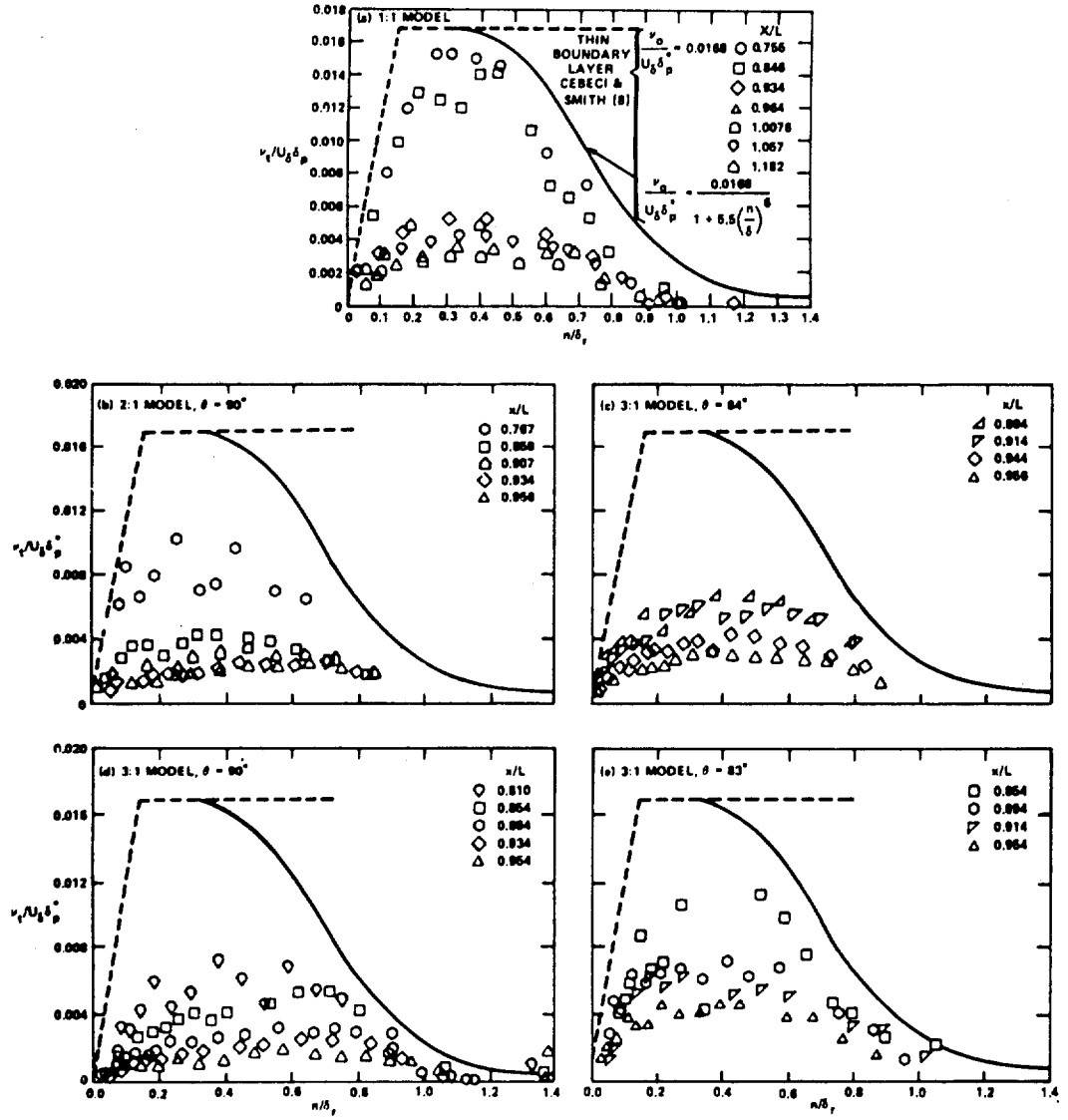

Figure 6 - Measured Distribution of Eddy Viscosity

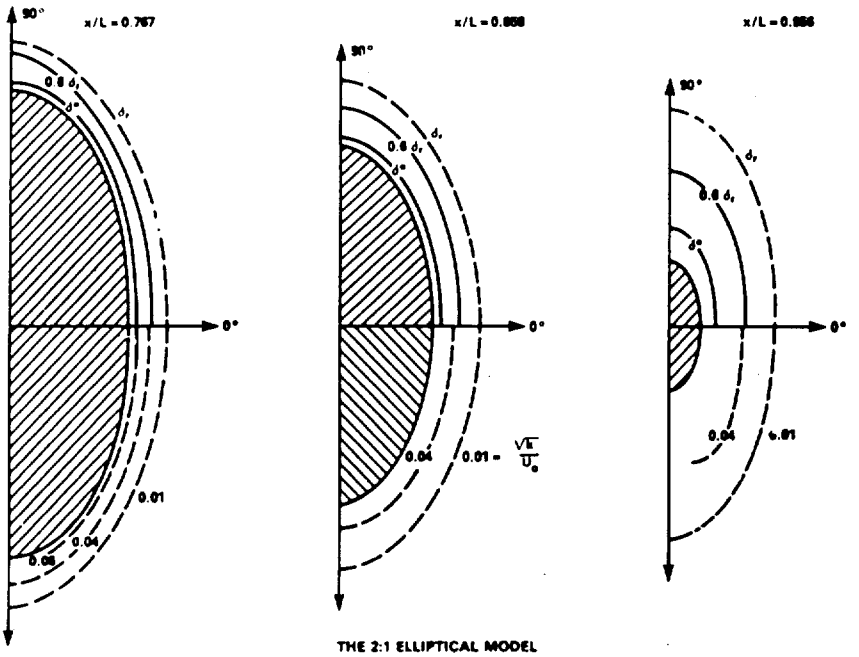

Figure 7 - Representing the Mixing Length of the Stern Flow by the Square Root of Turbulence Area

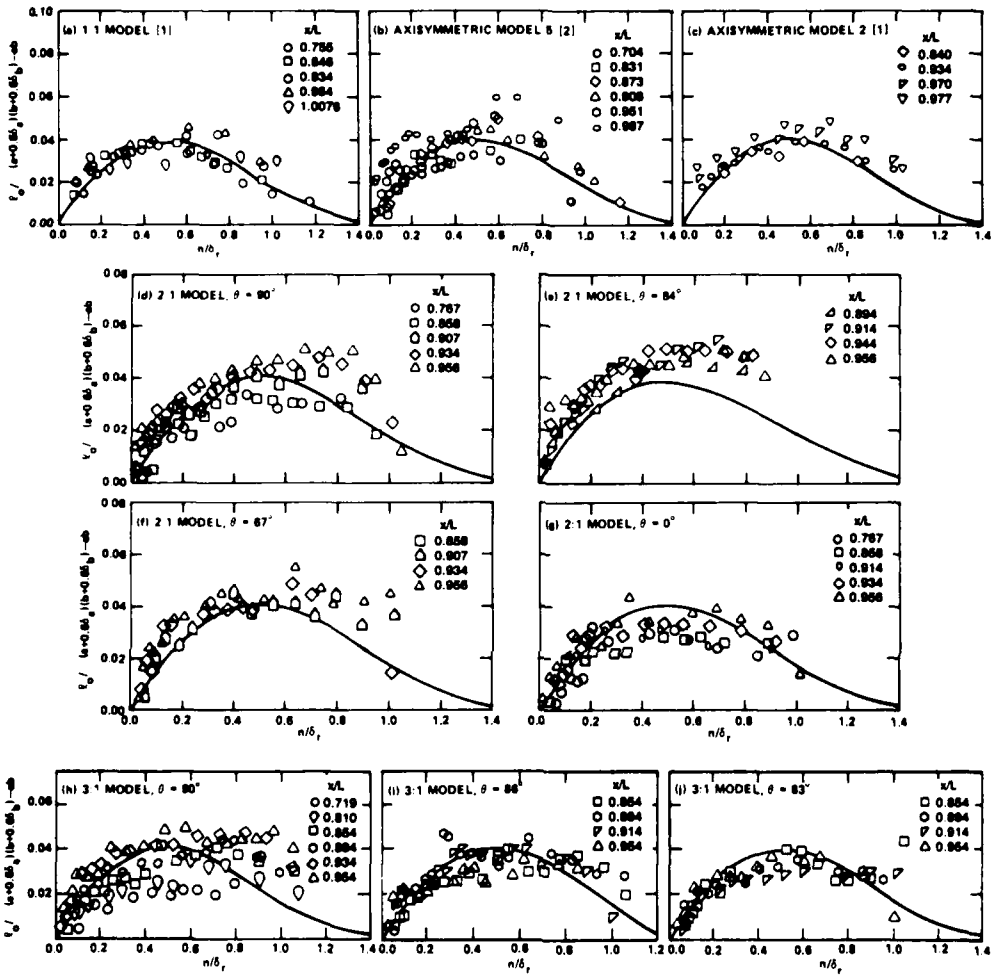

Figure 8 - Similarity Property of Mixing Length for Turbulent Stern Flows

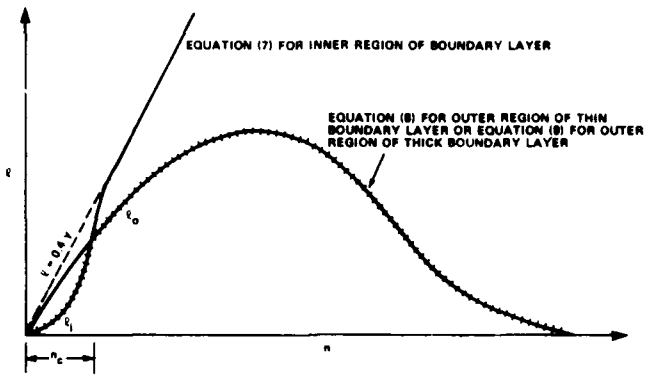

Figure 9 - Schematic of Mixing Length across the Boundary Layer

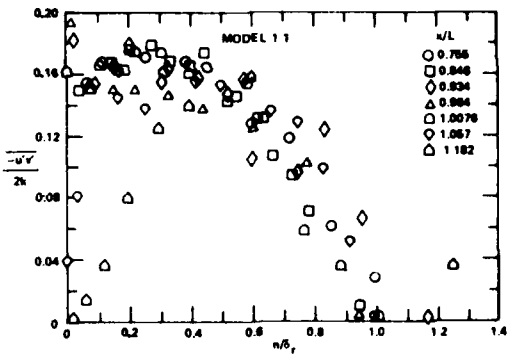

Figure 10 - Measured Distribution of Turbulent Structure Parameter

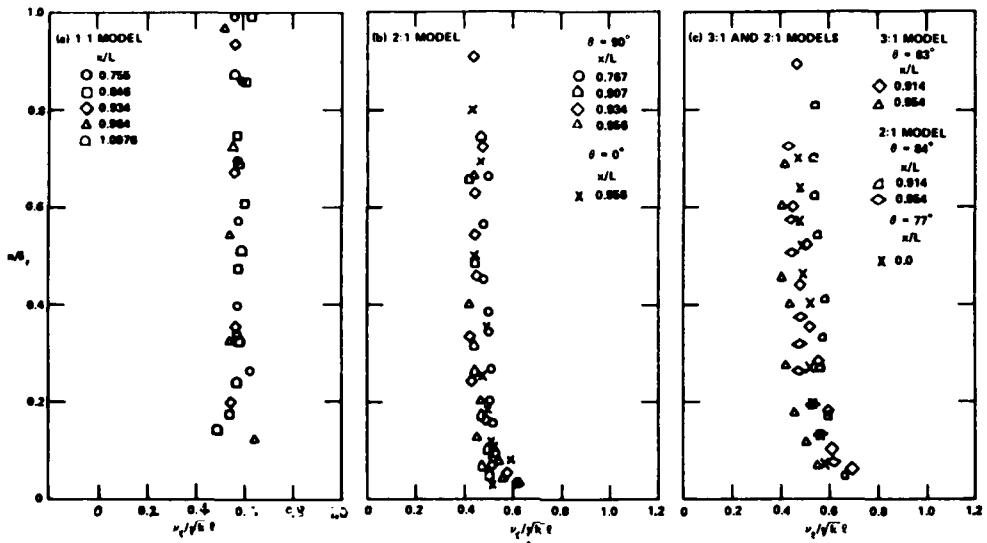

Figure 11 - The Constancy of the Measured Values of $\nu_t/\sqrt{k}\,\ell$ across the Thick Boundary Layers

x/L	y/L	x/L	y/L	x/L	y/L
0.0000	0.0000	0.2684	0.0456	0.7363	0.0427
0.0050	0.0100	0.2783	0.0456	0.7477	0.0421
0.0099	0.0142	0.2883	0.0456	0.7553	0.0416
0.0149	0.0175	0.2982	0.0456	0.7666	0.0408
0.0199	0.0202	0.3082	0.0456	0.7780	0.0399
0.0249	0.0227	0.3181	0.0456	0.7856	0.0392
0.0298	0.0248	0.3280	0.0456	0.7970	0.0382
0.0348	0.0268	0.3380	0.0456	0.8045	0.0375
0.0398	0.0287	0.3479	0.0456	0.8159	0.0363
0.0447	0.0303	0.3579	0.0456	0.8273	0.0350
0.0497	0.0319	0.3678	0.0456	0.8349	0.0341
0.0547	0.0333	0.3777	0.0456	0.8462	0.0326
0.0596	0.0347	0.3877	0.0456	0.8576	0.0310
0.0646	0.0359	0.3976	0.0456	0.8652	0.0299
0.0696	0.0370	0.4076	0.0456	0.8765	0.0281
0.0746	0.0381	0.4175	0.0456	0.8841	0.0268
0.0795	0.0390	0.4274	0.0456	0.8955	0.0248
0.0845	0.0399	0.4374	0.0456	0.9069	0.0226
0.0895	0.0407	0.4473	0.0456	0.9144	0.0211
0.0944	0.0414	0.4573	0.0456	0.9245	0.0189
0.0994	0.0421	0.4672	0.0456	0.9344	0.0166
0.1044	0.0427	0.4771	0.0456	0.9443	0.0140
0.1093	0.0432	0.4871	0.0456	0.9513	0.0122
0.1143	0.0437	0.4970	0.0456	0.9563	0.0108
0.1193	0.0441	0.5070	0.0456	0.9612	0.0095
0.1243	0.0444	0.5169	0.0456	0.9642	0.0087
0.1292	0.0447	0.5268	0.0456	0.9662	0.0081
0.1342	0.0450	0.5368	0.0456	0.9682	0.0076
0.1392	0.0452	0.5467	0.0456	0.9692	0.0074
0.1441	0.0453	0.5567	0.0456	0.9702	0.0072
0.1491	0.0454	0.5666	0.0456	0.9722	0.0068
0.1541	0.0455	0.5765	0.0456	0.9732	0.0066
0.1590	0.0456	0.5865	0.0456	0.9751	0.0063
0.1640	0.0456	0.5964	0.0456	0.9771	0.0062
0.1690	0.0456	0.6064	0.0456	0.9791	0.0059
0.1740	0.0456	0.6186	0.0456	0.9811	0.0056
0.1789	0.0456	0.6264	0.0455	0.9831	0.0053
0.1839	0.0456	0.6378	0.0455	0.9851	0.0050
0.1889	0.0456	0.6454	0.0455	0.9871	0.0048
0.1938	0.0456	0.6567	0.0453	0.9881	0.0046
0.1988	0.0456	0.6681	0.0452	0.9901	0.0043
0.2087	0.0456	0.6757	0.0450	0.9920	0.0040
0.2187	0.0456	0.6871	0.0448	0.9940	0.0036
0.2286	0.0456	0.6984	0.0444	0.9960	0.0028
0.2386	0.0456	0.7060	0.0441	0.9980	0.0019
0.2485	0.0456	0.7174	0.0437	1.0000	0.0000
0.2584	0.0456	0.7250	0.0433		

TABLE 1 - Offset of DTNSRDC Axisymmetric Model 1

INITIAL DISTRIBUTION

Copies	
1	WES
1	U.S. ARMY TRANS R&D Marine Trans Div
3	ONR/432F Whitehead, Lee, Reischman
1	ONR/Boston
1	ONR/Chicago
1	ONR/New York
1	ONR/Pasadena
1	ONR/San Francisco
2	NRL 1 Code 2027 1 Code 2629
1	NORDA
3	USNA 1 Tech Lib 1 Nav Sys Eng Dept 1 B. Johnson
3	NAVPGSCOL 1 Lib 1 T. Sarpkaya 1 J. Miller
1	NOSC/Lib
1	NCSC/712
1	NCEL/131
1	NSWC, White Oak/Lib
1	NSWC, Dahlgren/Lib
1	NUSC/Lib

Copies	
11	NAVSEA 1 SEA 05R24 (J. Sejd) 1 SEA 55W3 (E. Comstock) 1 SEA 55W33 (W. Sandburg) 1 SEA 55W31 (W. Louis) 1 SEA 55W31 (G. Jones) 1 SEA 55N2 (A. Paladino) 1 SEA 55N1 (S.G. Wieczorek) 1 SEA 63R31 (T. Peirce) 1 SEA 56X12 (C.R. Crockett) 1 SEA 62R41 (L. Pasiuk) 1 SEA 99612 (Library)
1	NAVFAC/032C
1	NADC
1	NAVSHIPYD PTSMH/Lib
1	NAVSHIPYD PHILA/Lib
1	NAVSHIPYD NORVA/Lib
1	NAVSHIPYD CHASN/Lib
1	NAVSHIPYD LBEACH/Lib
2	NAVSHIPYD MARE 1 Lib 1 Code 250
1	NAVSHIPYD PUGET/Lib
1	NAVSHIPYD PEARL/Code 202.32
1	NAVSEC, NORVA/6660.03, Blount
12	DTIC
1	AFOSR/NAM
1	AFFOL/FYS, J. Olsen
2	MARAD 1 Div of Ship R&D 1 Lib

Copies	
1	NASA/HQ/Lib
3	NASA/Ames Res Ctr, Lib 1 D. Kwak 1 J.L. Steger 1 Lib
2	NASA/Langley Res Ctr 1 Lib 1 D. Bushnell
1	NBS/Lib
1	LC/Sci & Tech
1	DOT/Lib TAD-491.1
1	MMA 1 National Maritime Res Ctr 1 Lib
3	U of Cal/Dept Naval Arch, Berkeley 1 Lib 1 W. Webster 1 R. Yeung
2	U of Cal, San Diego 1 A.T. Ellis 1 Scripps Inst Lib
1	U of Cal, Santa Barbara/Tulin
4	CIT 1 Aero Lib 1 T.Y. Wu 1 A.J. Acosta 1 D. Coles
1	California State University/ Cebeci
1	Catholic U of Amer/Civil & Mech Eng
1	Colorado State U/Eng Res Ctr
1	Cornell U/Shen

Copies	
2	Harvard U 1 G. Carrier 1 Gordon McKay Lib
1	U of Illinois/J. Robertson
4	U of Iowa 1 Lib 1 L. Landweber 1 V.C. Patel 1 C.J. Chen
1	Johns Hopkins U/Lib
4	MIT 1 Lib 1 J.R. Kerwin 1 T.F. Ogilvie 1 J.N. Newman
2	U of Minn/St. Anthony Falls 1 Lib 1 Arndt
1	U of Mich/NAME/Lib
1	U of Notre Dame/Eng Lib
1	New York U/Courant Inst/Lib
3	Penn State 1 B.R. Parkin 1 R.E. Henderson 1 ARL Lib
1	Princeton U/Mellor
1	U of Rhode Island/F.M. White
1	Science Application, Inc. Annapolis, MD C. von Kerczek
1	SIT/Lib
1	U of Texas/Arl Lib
1	Utah State U/Jeppson

Copies	
1	Southwest Res Inst 1 Applied Mech Rev
3	Stanford U 1 Eng Lib 1 R. Street, Dept Civil Eng 1 S.J. Kline, Dept Mech Eng
1	Stanford Res Inst/Lib
1	U of Virginia/Aero Eng Dept
1	U of Washington/Arl Tech Lib
2	VPI 1 Dept of Mech Eng 1 J. Schetz, Dept Aero & Ocean Eng
2	Webb Inst 1 Lib 1 Ward
1	Woods Hole/Ocean Eng
1	Worchester PI/Tech Lib
1	SNAME/Tech Lib
1	Bell Aerospace
1	Bethlehem Steel/Sparrows Point
1	National Science Foundation/ Eng Div Lib
1	Bethlehem Steel/New York/Lib
4	Boeing Company/Seattle 1 Marine System 1 P. Rubbert 1 G. Paynter 1 H. Yoshihara
1	Bolt, Beranek & Newman/Lib
1	Cambridge Acoustical Associates, Inc.
1	Exxon, NY/Design Div/ Tank Dept

Copies	
1	Exxon Math & System, Inc.
1	General Dynamics, EB/ Boatwright
1	Flow Research
1	Gibbs & Cox/Tech Info
2	Grumman Aerospace Corp 1 Lib 1 R.E. Melnik
1	Hydronautics/Lib
1	Lockheed, Sunnyvale/Waid
1	Lockheed, California/Lib
1	Lockheed, Georgia/Lib
2	McDonnell Douglas, Long Beach 1 T. Cebeci 1 J.L. Hess
1	Newport News Shipbuilding/Lib
1	Nielsen Eng & Research
1	Northrop Corp/Aircraft Div
1	Rand Corp
1	Rockwell International 1 B. Ujihara
1	Sperry Rand/Tech Lib
1	Sun Shipbuilding/Chief Naval Arch
1	TRW Systems Group/Lib
1	TRACOR
1	United Technology/East Hartford, Conn
2	Westinghouse Electric 1 M.S. Macovsky 1 Gulino

CENTER DISTRIBUTION

Copies	Code	Name
1	012.3	D.D. Moran
1	1500	W.B. Morgan
1	1504	V.J. Monacella
1	1506	S. Hawkins
1	1508	R. Boswell
1	152	W.C. Lin
1	1521	W. Day
1	1522	C.C. Hsu
1	1522	M.B. Wilson
1	1522	C.H. Sung
1	154	J. McCarthy
1	154	P. Granville
1	1540.1	B. Yim
1	1540.2	R. Cumming
30	1542	T.T. Huang
1	1542	N.C. Groves
1	1542	G.S. Belt
1	1542	Y.T. Lee
1	1542	M.S. Chang
1	1542	R.W. Burke
1	1544	F. Peterson
1	156	D.S. Cieslowski
1	1561	G. Cox
1	1564	J. Feldman
1	1606	T.C. Tai
1	1802.1	H. Lugt
1	1840	J. Schot
1	1843	H. Haussling
1	19	M.M. Sevik
1	1905.1	W. Blake
1	194	F.S. Archibald
10	5211.1	Reports Distribution
1	522.1	TIC (C)
1	522.2	TIC (A)

DTNSRDC ISSUES THREE TYPES OF REPORTS

1. DTNSRDC REPORTS, A FORMAL SERIES, CONTAIN INFORMATION OF PERMANENT TECHNICAL VALUE. THEY CARRY A CONSECUTIVE NUMERICAL IDENTIFICATION REGARDLESS OF THEIR CLASSIFICATION OR THE ORIGINATING DEPARTMENT.

2. DEPARTMENTAL REPORTS, A SEMIFORMAL SERIES, CONTAIN INFORMATION OF A PRELIMINARY, TEMPORARY, OR PROPRIETARY NATURE OR OF LIMITED INTEREST OR SIGNIFICANCE. THEY CARRY A DEPARTMENTAL ALPHANUMERICAL IDENTIFICATION.

3. TECHNICAL MEMORANDA, AN INFORMAL SERIES, CONTAIN TECHNICAL DOCUMENTATION OF LIMITED USE AND INTEREST. THEY ARE PRIMARILY WORKING PAPERS INTENDED FOR INTERNAL USE. THEY CARRY AN IDENTIFYING NUMBER WHICH INDICATES THEIR TYPE AND THE NUMERICAL CODE OF THE ORIGINATING DEPARTMENT. ANY DISTRIBUTION OUTSIDE DTNSRDC MUST BE APPROVED BY THE HEAD OF THE ORIGINATING DEPARTMENT ON A CASE-BY-CASE BASIS.